Supplemental Information:

Carbon content drives high temperature superconductivity in a carbonaceous sulfur hydride below 1 Mbar

G. Alexander Smith,[1,2] Ines E. Collings,[3] Elliot Snider,[4] Dean Smith,[1] Sylvain Petitgirard,[5] Jesse Smith,[6] Melanie White,[1,7] Elyse Jones,[4] Paul Ellison,[7] Keith V. Lawler,[1] Ranga P. Dias,[4,8] and Ashkan Salamat[1,7,*]

[1]*Nevada Extreme Conditions Laboratory, University of Nevada, Las Vegas, Las Vegas, Nevada, 89154, USA*

[2]*Department of Chemistry & Biochemistry, University of Nevada, Las Vegas, Las Vegas, Nevada 89154, USA*

[3]*Centre for X-ray Analytics, Empa Swiss Federal Laboratories for Materials Science and Technology, ÜberlandstraSSe 129, 8600 Dübendorf, Switzerland.*

[4]*Department of Mechanical Engineering, University of Rochester, Rochester, New York 14627, USA*

[5]*Department of Earth Sciences, ETH Zürich, Zürich 8025, Switzerland*

[6]*HPCAT, X-ray Science Division, Argonne National Laboratory, Illinois 60439, USA*

[7]*Department of Physics & Astronomy, University of Nevada, Las Vegas, Las Vegas, Nevada 89154, USA*

[8]*Department of Physics & Astronomy, University of Rochester, Rochester, New York 14627, USA*

(Dated: July 5, 2022)

C-S-H SYNTHESIS

We conducted an independent study to that of Snider *et al.* [1], with the synthesis of 11 crystals of C-S-H carried out at UNLV. Boehler-Almax design diamonds with 80° apertures were used in conjunction with modified BX90 style cells to enable a higher degree of completeness in the acquisition of SC-XRD data. Each cell was prepared using Re foil as a gasket material, which was preindented to a 10th of the culet diameter, confirmed using interferometry, and a sample chamber made by laser micromachining. A sample of a ball-milled mixture of elemental carbon and sulfur with dimensions about 15% of the diamond culet was placed into the sample chamber, as well as a ruby sphere to accurately determine pressures below 10 GPa.[2] Gas-phase H_2 was loaded at 3 kbar.[3] Samples were then pressurized to 3.7–4.0 GPa and excited for several hours using a 514 nm laser with power ranging from 10 and 150 mW depending on sample response. As the sulfur bond is photochemically cleaved using green laser, the sample will begin to appear transparent, after this point sulfur will have a tendency to form the van der Waal crystal. At this point focusing higher powered laser on the carbon sample for several hours, often overnight at the highest available power available, to warm carbon in a liquid hydrogen medium will help react carbon into the CSH crystal. After pressing above the solidification of hydrogen, rapid small crystal formation will grow. At this stage the crystal is still sensitive to higher laser powers and can be manipulated, albeit, they are much less volatile, to help place and form a single crystal. Without unreacted carbon, leads, or ruby in the chamber, it is often very difficult to place the crystal in an ideal position. After synthesis crystals were pressed to about 10 GPa to ensure stability during Raman. Raman spectroscopy was used to confirm the transformation into CSH *via* the previously reported C-H, S-H, and H-H Raman modes at ∼4 GPa.[1]

EXPERIMENTALLY DETERMINED BIRCH-MURNAGHAN EQUATION OF STATE FITS

Presented below are the fit parameters for the 2nd-order Birch-Murnaghan equation of state.

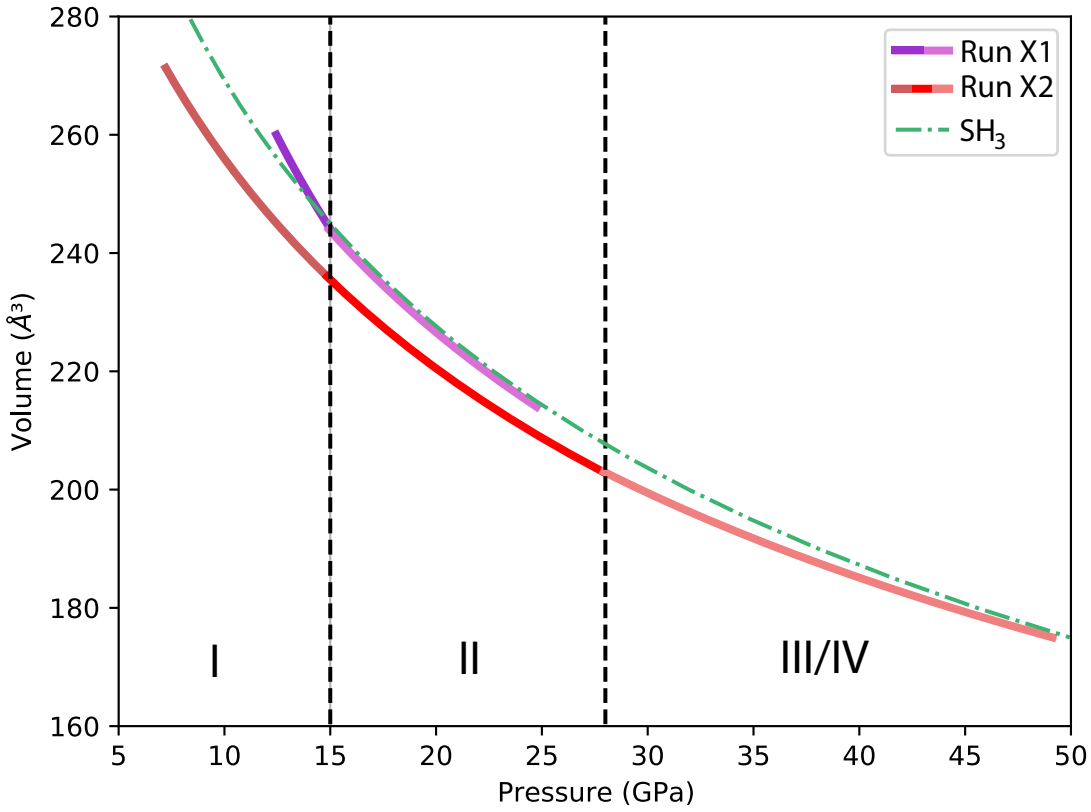

Figure S1: A plot of the representation of fitted results. Plotted results are presented from first measured point to the either the next phase or highest pressure for a given run. The presented phase boundaries are from the boundaries determined from SC-XRD in this work.

Table SI: The fit parameters of the 2nd Order Birch-Murnaghan equation of state fits. Phase III/IV contributions were determined from fits to both crystals 3 and 4 from Run X2.

Run X1	Crystal	K_0 (GPa)	V_0 (Å^3)
	1	8.39	434.76
	2	10.02	412.80
	3	7.32	448.69
	Phase I	1.32	761.55
	Phase II	11.67	395.96
	All	8.40	433.16
Run X2	Crystal	K_0 (GPa)	V_0 (Å^3)
	1	13.75	377.29
	2	13.19	377.60
	3	14.50	372.87
	4	13.08	378.77
	Phase I	1.01	791.54
	Phase II	17.31	349.00
	Phase III/IV	21.32	331.31
	All	13.09	380.68
Full Data Set		K_0 (GPa)	V_0 (Å^3)
	Phase I	6.32	464.21
	Phase II	4.86	504.29
	Phase III/IV	21.32	331.31
	All	11.32	397.54
SH_3	Crystal	K_0 (GPa)	V_0 (Å^3)
	all	11.44	399.75

SC-XRD DETERMINED STRUCTURES

Single-crystal Xray diffraction experiments were performed at the HPCAT beamline using monochromatic Xrays with the wavelength of 0.3445 Å. The Xray beam was focused to 2.4 μm by 6.4 μm. Diffraction images were collected using a Pilatus 1M detector detector. The beamline parameters were calibrated with CeO_2 powder and an enstatite single crystal using the programs Dioptas and CrysAlisPro, respectively.[4, 5] Data collections were performed using step scans of 0.5° with 3-5 s exposure over a total ω scan range of ±30° (DAC1) and ±35° (DAC2) about the vertical axis of the DAC. The lattice parameters and the integrated intensities of the Bragg reflections were obtained from the measured images using the program CrysAlisPro.[5] The crystal structures of CSH were solved using direct methods implemented in the SHELXT program.[6] The iterative structure refinements were performed with the SHELXL program[7] built in the ShelXle graphical user interface.[8] Details on the crystal structure refinements are given in Tables SVI-XVIII. Three $(CH_4)_x(H_2S)_{2-x}H_2$ loadings (DAC1, DAC2, and DAC4) used in this study, and a $(H_2S)_2H_2$ loading (DAC3) are shown in Figure S2. Figures S3-9 show the reciprocal space reconstructions for the different crystals in the four loadings. These highlight that the crystal quality can vary, as well as the occurrence of the monoclinic distortion.

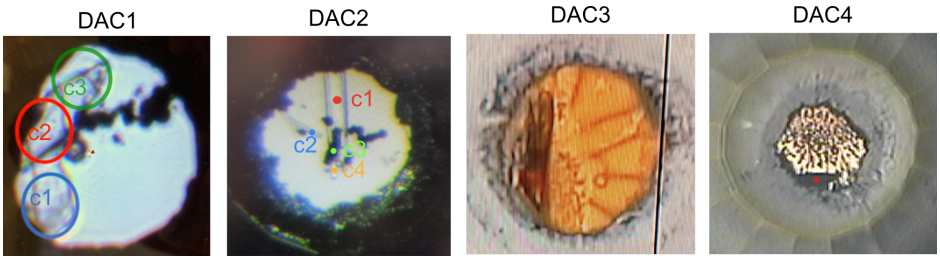

Figure S2: Diamond-anvil sample chambers for experiments 1-4.

$(CH_4)_x(H_2S)_{2-x}H_2$ DAC1

Table SII: Crystallographic details of $(CH_4)_x(H_2S)_{2-x}H_2$ at variable pressure for c1 in DAC1.

P (GPa)	12.2	14.4	15.0	16.1	17.2	18.8
Crystal System	Tetragonal					
Space Group	$I4/mcm$					
Z	8					
a (Å)	6.8228(13)	6.695(2)	6.661(3)	6.613(2)	6.5691(18)	6.516(3)
c (Å)	5.6283(14)	5.552(2)	5.536(3)	5.507(3)	5.481(2)	5.450(3)
V (Å^3)	262.00(12)	248.91(19)	245.6(2)	240.8(2)	236.50(16)	231.4(2)
Data collection						
No. of reflections						
measured	234	264	273	267	204	223
unique	87	75	80	78	65	70
unique with I $> 2\sigma$	71	62	66	63	53	57
R_{int}	0.0507	0.0187	0.0182	0.0491	0.0573	0.0606
Refinement						
No. of parameters	10	11	9	9	9	9
No. of restraints	4	4	4	4	4	4
Data/parameter ratio	7.5	6.0	7.8	7.4	6.3	6.8
R_1 $[I > 2\sigma(I)]$	0.0585	0.0484	0.0576	0.046	0.0437	0.0547
wR_2 (all data)	0.1847	0.1432	0.1691	0.1237	0.1284	0.1328
$\Delta\rho_{min}/\Delta\rho_{max}$ (eÅ^{-3})	0.46/-0.63	0.47/-0.48	0.69/-0.74	0.51/-0.56	0.45/-0.43	0.56/-0.55

Table SIII: Crystallographic details of $(CH_4)_x(H_2S)_{2-x}H_2$ at variable pressure for c1 in DAC1.

P (GPa)	20.3	22.4	24.5
Crystal System	Monoclinic		
Space Group	$C2/c$		
Z	24		
a (Å)	8.458(2)	8.404(4)	8.316(4)
b (Å)	6.5003(17)	6.452(3)	6.419(3)
c (Å)	12.504(4)	12.409(7)	12.246(9)
β (°)	99.58(3)	99.56(5)	99.57(6)
V (Å^3)	677.8(3)	663.5(6)	644.5(6)
Data collection			
No. of reflections			
measured	708	680	643
unique	486	474	456
unique with I $> 2\sigma$	285	288	243
R_{int}	0.0156	0.019	0.0252
Refinement			
No. of parameters	56	56	57
No. of restraints	11	10	11
Data/parameter ratio	5.3	5.3	4.5
R_1 $[I > 2\sigma(I)]$	0.0552	0.0685	0.0953
wR_2 (all data)	0.2147	0.2222	0.3524
$\Delta\rho_{min}/\Delta\rho_{max}$ (eÅ^{-3})	0.62/-0.53	0.57/-0.54	1.30/-0.75

Table SIV: Crystallographic details of $(CH_4)_x(H_2S)_{2-x}H_2$ at variable pressure for c2 in DAC1.

P (GPa)	12.2	14.4	15.0	16.1	17.2
Crystal System	Tetragonal				
Space Group	$I4/mcm$				
Z	8				
a (Å)	6.8028(9)	6.667(3)	6.639(4)	6.594(5)	6.539(6)
c (Å)	5.6337(10)	5.564(2)	5.543(3)	5.509(3)	5.488(4)
V (Å^3)	260.72(8)	247.3(3)	244.3(3)	239.5(4)	234.7(5)
Data collection					
No. of reflections					
measured	250	254	253	234	180
unique	96	94	93	91	76
unique with I $> 2\sigma$	80	80	80	75	54
R_{int}	0.0199	0.0544	0.0762	0.009	0.0198
Refinement					
No. of parameters	9	11	9	5	5
No. of restraints	4	3	3	1	1
Data/parameter ratio	9.3	7.5	9.2	15.2	11.0
R_1 $[I > 2\sigma(I)]$	0.0849	0.0424	0.066	0.0837	0.0872
wR_2 (all data)	0.1815	0.1146	0.1719	0.2074	0.2862
$\Delta\rho_{min}/\Delta\rho_{max}$ (eÅ^{-3})	0.90/-0.94	0.50/-0.49	0.90/-0.65	1.60/-1.07	0.65/-0.71

Table SV: Crystallographic details of $(CH_4)_x(H_2S)_{2-x}H_2$ at variable pressure for c2 in DAC1.

P (GPa)	18.8	20.3	22.4	24.5
Crystal System	Monoclinic			
Space Group	$C2/c$			
Z	24			
a (Å)	8.567(8)	8.500(8)	8.417(7)	8.311(11)
b (Å)	6.531(4)	6.495(3)	6.457(3)	6.393(5)
c (Å)	12.512(8)	12.410(7)	12.354(9)	12.303(12)
β (°)	99.52(8)	99.50(7)	99.54(8)	99.44(11)
V (Å^3)	690.3(9)	675.8(8)	662.0(8)	644.9(12)
Data collection				
No. of reflections				
measured	710	681	685	672
unique	431	425	433	435
unique with I $> 2\sigma$	289	262	276	232
R_{int}	0.0676	0.0238	0.0667	0.03
Refinement				
No. of parameters	53	35	28	28
No. of restraints	10	0	0	0
Data/parameter ratio	5.6	7.5	9.9	8.3
R_1 $[I > 2\sigma(I)]$	0.1129	0.0849	0.0886	0.0856
wR_2 (all data)	0.4069	0.2639	0.2933	0.2744
$\Delta\rho_{min}/\Delta\rho_{max}$ (eÅ^{-3})	2.07/-1.04	0.95/-0.79	0.95/-0.81	1.23/-0.73

Table SVI: Crystallographic details of $(CH_4)_x(H_2S)_{2-x}H_2$ at variable pressure for c3 in DAC1.

P (GPa)	12.2	14.4	15.0	16.1	17.2
Crystal System	Tetragonal				
Space Group	$I4/mcm$				
Z	8				
a (Å)	6.8236(10)	6.6883(13)	6.658(3)	6.618(3)	6.575(2)
c (Å)	5.6430(9)	5.5276(9)	5.5008(14)	5.4500(14)	5.4358(14)
V (Å^3)	262.75(9)	247.27(10)	243.9(2)	238.7(2)	235.01(17)
Data collection					
No. of reflections					
measured	261	253	226	206	167
unique	97	93	91	76	71
unique with I $> 2\sigma$	84	79	77	58	49
R_{int}	0.0148	0.0835	0.0555	0.1006	0.0306
Refinement					
No. of parameters	10	9	8	8	9
No. of restraints	4	4	4	4	4
Data/parameter ratio	8.4	8.8	9.6	7.3	5.4
R_1 $[I > 2\sigma(I)]$	0.0262	0.0525	0.0569	0.0717	0.1105
wR_2 (all data)	0.0758	0.1365	0.1487	0.2116	0.3815
$\Delta\rho_{min}/\Delta\rho_{max}$ (eÅ^{-3})	0.24/−0.22	0.67/−0.78	0.53/−0.69	0.57/−0.47	0.88/−1.35

Table SVII: Crystallographic details of $(CH_4)_x(H_2S)_{2-x}H_2$ at variable pressure for c3 in DAC1.

P (GPa)	18.8	20.3	22.4	24.5
Crystal System	Monoclinic			
Space Group	$C2/c$			
Z	24			
a (Å)	8.457(3)	8.394(3)	8.337(3)	8.257(3)
b (Å)	6.5590(14)	6.5180(19)	6.4877(12)	6.4271(17)
c (Å)	12.562(4)	12.458(5)	12.317(4)	12.194(5)
β (°)	98.81(4)	98.81(5)	98.72(3)	98.69(4)
V (Å^3)	688.7(4)	673.6(4)	658.5(3)	639.7(4)
Data collection				
No. of reflections				
measured	678	646	635	618
unique	432	415	411	401
unique with I $> 2\sigma$	315	272	256	251
R_{int}	0.0475	0.0720	0.0914	0.1087
Refinement				
No. of parameters	50	50	46	50
No. of restraints	9	9	9	9
Data/parameter ratio	6.3	5.4	5.6	5.0
R_1 $[I > 2\sigma(I)]$	0.0788	0.0871	0.0919	0.0885
wR_2 (all data)	0.2875	0.3033	0.2932	0.2795
$\Delta\rho_{min}/\Delta\rho_{max}$ (eÅ^{-3})	0.65/−0.90	0.69/−0.78	0.66/−0.55	0.85/−0.69

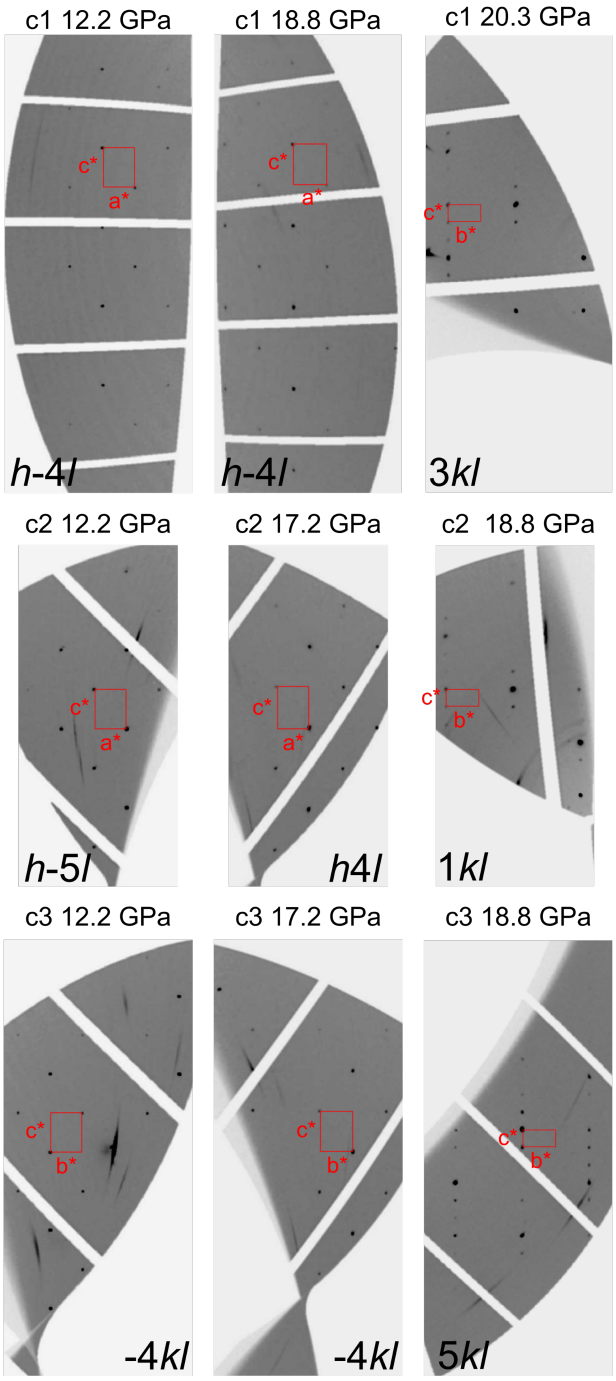

Figure S3: Selected reciprocal space reconstructions for crystals 1 to 3 of the $(CH_4)_x(H_2S)_{2-x}H_2$ loading in DAC1. The monoclinic phase is observed for all crystals at 19-20 GPa.

$(CH_4)_x(H_2S)_{2-x}H_2$ DAC2

Table SVIII: Crystallographic details of $(CH_4)_x(H_2S)_{2-x}H_2$ at variable pressure for c1 in DAC2.

P (GPa)	8	9	13	18	26	29
Crystal System	Tetragonal					
Space Group	$I4/mcm$					
Z	8					
a (Å)	7.099(7)	6.863(10)	6.654(10)	6.480(6)	6.35(3)	6.275(6)
c (Å)	5.859(2)	5.734(7)	5.566(7)	5.400(3)	5.189(10)	5.238(3)
V (Å^3)	295.3(6)	270.1(9)	246.4(8)	226.7(4)	209(2)	206.3(4)
Data collection						
No. of reflections						
measured	360	351	302	279	281	266
unique	114	108	90	87	81	78
unique with I $> 2\sigma$	52	57	52	58	43	44
R_{int}	0.0432	0.0375	0.1805	0.033	0.1433	0.0507
Refinement						
No. of parameters	6	3	4	7	4	4
No. of restraints	0	0	0	0	0	0
Data/parameter ratio	8.7	19.0	13.0	8.3	10.8	11.0
R_1 $[I > 2\sigma(I)]$	0.1285	0.1249	0.1031	0.1221	0.1618	0.1149
wR_2 (all data)	0.3585	0.329	0.2744	0.2851	0.3582	0.2914
$\Delta\rho_{min}/\Delta\rho_{max}$ (eÅ^{-3})	0.81/-1.48	1.07/-0.62	1.03/-0.54	1.02/-0.89	1.22/-0.70	0.72/-0.58

Table SIX: Crystallographic details of $(CH_4)_x(H_2S)_{2-x}H_2$ at variable pressure for c1 in DAC2.

P (GPa)	32	37	38	40	45	49
Crystal System	Tetragonal					
Space Group	$I4/mcm$					
Z	8					
a (Å)	6.221(5)	6.124(3)	6.094(3)	6.072(2)	5.976(5)	6.022(10)
c (Å)	5.179(2)	5.135(2)	5.1148(16)	5.0961(11)	5.011(5)	5.011(8)
V (Å^3)	200.4(3)	192.6(2)	189.94(18)	187.91(15)	179.0(3)	181.7(7)
Data collection						
No. of reflections						
measured	270	251	256	214	240	218
unique	80	74	73	70	82	83
unique with I $> 2\sigma$	54	64	64	60	31	25
R_{int}	0.0344	0.0177	0.0242	0.0667	0.1459	0.1798
Refinement						
No. of parameters	4	3	3	4	7	3
No. of restraints	0	0	0	0	0	0
Data/parameter ratio	13.5	21.3	21.3	15.0	4.4	8.3
R_1 $[I > 2\sigma(I)]$	0.1105	0.0922	0.1146	0.087	0.1518	0.1768
wR_2 (all data)	0.2716	0.2288	0.2657	0.1962	0.3636	0.4235
$\Delta\rho_{min}/\Delta\rho_{max}$ (eÅ^{-3})	0.98/-0.98	1.29/-0.87	1.28/-0.87	0.66/-0.93	1.05/-0.82	1.36/-0.73

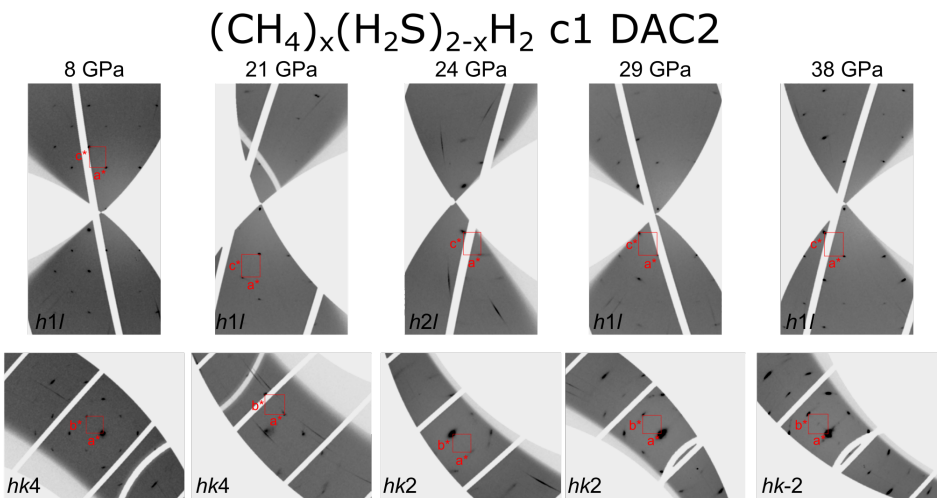

Figure S4: Selected reciprocal space reconstructions for crystal 1 of the $(CH_4)_x(H_2S)_{2-x}H_2$ loading in DAC2. No monoclinic distortion is observed in this crystal. The diffraction spots have a large mosaicity in the **ab**-plane.

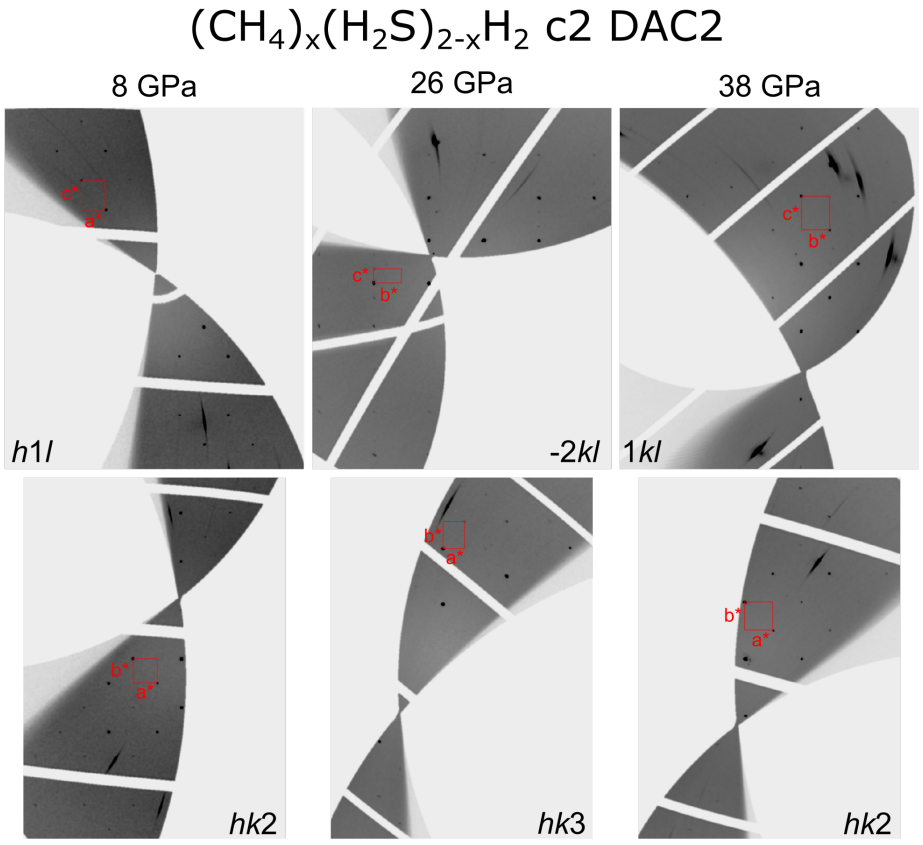

Figure S5: Selected reciprocal space reconstructions for crystal 2 of the $(CH_4)_x(H_2S)_{2-x}H_2$ loading in DAC2. The monoclinic distortion is observed at pressure points 24 and 26 GPa.

Table SX: Crystallographic details of $(CH_4)_x(H_2S)_{2-x}H_2$ at variable pressure for c2 in DAC2.

P (GPa)	8	9	18	29	32
Crystal System	Tetragonal				
Space Group	$I4/mcm$				
Z	8				
a (Å)	7.0808(18)	6.8963(14)	6.4685(10)	6.2150(9)	6.1810(10)
c (Å)	5.8513(16)	5.6994(13)	5.3946(9)	5.2094(7)	5.1719(6)
V (Å^3)	293.37(17)	271.06(13)	225.72(8)	201.22(6)	197.59(7)
Data collection					
No. of reflections					
measured	430	362	229	264	263
unique	164	151	120	106	101
unique with I $> 2\sigma$	99	117	66	77	66
R_{int}	0.0392	0.0263	0.0802	0.1359	0.0348
Refinement					
No. of parameters	4	11	3	3	4
No. of restraints	0	2	0	0	0
Data/parameter ratio	24.8	10.6	22	25.7	16.5
R_1 $[I > 2\sigma(I)]$	0.0489	0.0470	0.1195	0.1066	0.0625
wR_2 (all data)	0.1444	0.1144	0.3279	0.3065	0.1822
$\Delta\rho_{min}/\Delta\rho_{max}$ (eÅ^{-3})	0.51/−0.48	0.50/−0.40	1.5/−1.9	1.4/−1.8	1.1/−1.4

Table SXI: Crystallographic details of $(CH_4)_x(H_2S)_{2-x}H_2$ at variable pressure for c2 in DAC2.

P (GPa)	24	26
Crystal System	Monoclinic	
Space Group	$C2/c$	
Z	24	
a (Å)	8.243(3)	8.180(4)
b (Å)	6.3158(6)	6.2688(9)
c (Å)	12.2764(15)	12.226(2)
β (°)	99.205(19)	99.26(3)
V (Å^3)	630.9(2)	618.8(3)
Data collection		
No. of reflections		
measured	980	947
unique	582	567
unique with I $> 2\sigma$	379	300
R_{int}	0.1888	0.0813
Refinement		
No. of parameters	13	53
No. of restraints	0	10
Data/parameter ratio	29	7.1
R_1 $[I > 2\sigma(I)]$	0.1629	0.0675
wR_2 (all data)	0.4371	0.2292
$\Delta\rho_{min}/\Delta\rho_{max}$ (eÅ^{-3})	2.0/−1.7	0.62/−0.68

Table SXII: Crystallographic details of $(CH_4)_x(H_2S)_{2-x}H_2$ at variable pressure for c2 in DAC2.

P (GPa)	37	38	40	45	49
Crystal System	Tetragonal				
Space Group	$I4/mcm$				
Z	8				
a (Å)	6.088(2)	6.068(2)	6.0509(19)	5.981(2)	5.974(3)
c (Å)	5.109(2)	5.089(2)	5.077(2)	5.007(2)	4.975(5)
V (Å^3)	189.35(16)	187.39(15)	185.88(14)	179.14(14)	177.5(2)
Data collection					
No. of reflections					
measured	240	239	233	223	175
unique	101	101	98	93	81
unique with I $> 2\sigma$	64	63	56	75	51
R_{int}	0.0774	0.0737	0.1139	0.0289	0.176
Refinement					
No. of parameters	3	3	12	11	
No. of restraints	0	0	0	0	
Data/parameter ratio	21.3	21.0	4.7	6.8	
R_1 $[I > 2\sigma(I)]$	0.1183	0.0887	0.1289	0.0834	
wR_2 (all data)	0.2863	0.2153	0.2643	0.1983	
$\Delta\rho_{min}/\Delta\rho_{max}$ (eÅ^{-3})	1.706/-1.33	1.228/-1.095	0.951/-1.193	1.486/-0.975	

Table SXIII: Crystallographic details of $(CH_4)_x(H_2S)_{2-x}H_2$ at variable pressure for c3 in DAC2.

P (GPa)	8	9	24	26	37
Crystal System	Tetragonal				
Space Group	$I4/mcm$				
Z	8				
a (Å)	7.079(4)	6.8889(10)	6.321(8)	6.297(3)	6.122(10)
c (Å)	5.850(2)	5.7016(8)	5.299(3)	5.260(2)	5.126(5)
V (Å^3)	293.1(4)	270.58(9)	211.7(5)	208.6(2)	192.1(7)
Data collection					
No. of reflections					
measured	393	371	290	285	259
unique	108	101	82	83	75
unique with I $> 2\sigma$	63	72	47	61	16
R_{int}	0.0585	0.0268	0.0403	0.1174	0.3467
Refinement					
No. of parameters	4	4	5	3	4
No. of restraints	0	0	1	0	0
Data/parameter ratio	15.8	18	9.4	20.3	4
R_1 $[I > 2\sigma(I)]$	0.1297	0.048	0.0719	0.0915	0.1309
wR_2 (all data)	0.2888	0.1371	0.1972	0.2333	0.4019
$\Delta\rho_{min}/\Delta\rho_{max}$ (eÅ^{-3})	0.63/-0.79	0.46/-0.35	0.54/-0.40	1.29/-0.73	0.56/-0.36

Table SXIV: Crystallographic details of $(CH_4)_x(H_2S)_{2-x}H_2$ at variable pressure for c3 in DAC2.

P (GPa)	18	29	32
Crystal System	Monoclinic		
Space Group	$C2/c$		
Z	24		
a (Å)	8.388(4)	8.152(5)	8.108(2)
b (Å)	6.498(5)	6.287(3)	6.251(2)
c (Å)	12.501(5)	12.141(7)	12.055(4)
β (°)	98.73(5)	99.00(6)	98.98(3)
V (Å^3)	673.4(6)	614.6(6)	603.5(3)
Data collection			
No. of reflections			
measured	1012	886	873
unique	633	578	564
unique with I $> 2\sigma$	267	301	329
R_{int}	0.1225	0.0584	0.1262
Refinement			
No. of parameters	13	13	13
No. of restraints	0	0	0
Data/parameter ratio	21	23	25
R_1 $[I > 2\sigma(I)]$	0.0919	0.1044	0.1348
wR_2 (all data)	0.2914	0.4093	0.4148
$\Delta\rho_{min}/\Delta\rho_{max}$ (eÅ^{-3})	0.89/-0.98	2.07/-1.73	2.09/-1.35

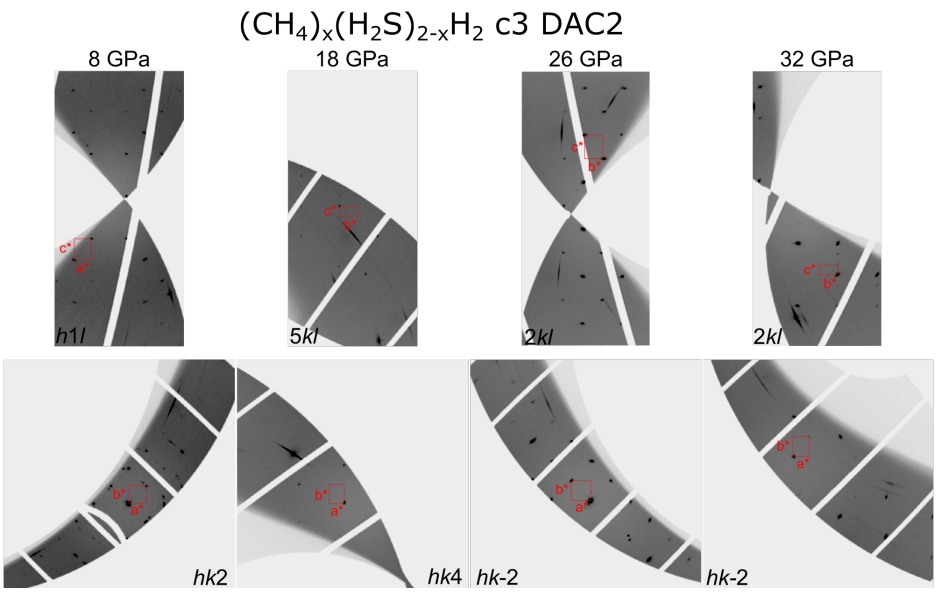

Figure S6: Selected reciprocal space reconstructions for crystal 3 of the $(CH_4)_x(H_2S)_{2-x}H_2$ loading in DAC2. The monoclinic distortion is observed at 18 GPa. The few reflections observed at 18 GPa is due to crystal alignment issues, which was fixed by re-defining its position after 24 GPa. Weak reflections of the monoclinic distortion are observed for pressure points 29 and 32 GPa.

Table SXV: Crystallographic details of $(CH_4)_x(H_2S)_{2-x}H_2$ at variable pressure for c4 in DAC2.

P (GPa)	8	9	24	26	29
Crystal System			Tetragonal		
Space Group			$I4/mcm$		
Z			8		
a (Å)	7.085(5)	6.893(2)	6.333(2)	6.25(3)	6.258(2)
c (Å)	5.853(3)	5.6925(15)	5.2304(11)	5.19(3)	5.1553(12)
V (Å^3)	293.8(4)	270.46(19)	209.79(15)	203(3)	201.90(16)
Data collection					
No. of reflections					
measured	374	368	259	288	281
unique	111	108	80	85	86
unique with I $> 2\sigma$	68	80	63	9	48
R_{int}	0.0706	0.0301	0.0308	0.8049	0.078
Refinement					
No. of parameters	4	8	3	3	4
No. of restraints	0	0	0	0	0
Data/parameter ratio	17	10	21	3	12
R_1 $[I > 2\sigma(I)]$	0.0456	0.0543	0.0963	0.2788	0.1384
wR_2 (all data)	0.161	0.1322	0.3053	0.7549	0.4008
$\Delta\rho_{min}/\Delta\rho_{max}$ (eÅ^{-3})	0.48/-0.42	0.46/-0.42	1.02/-1.55	0.74/-0.63	1.64/-1.31

Table SXVI: Crystallographic details of $(CH_4)_x(H_2S)_{2-x}H_2$ at variable pressure for c4 in DAC2.

P (GPa)	32	37	38	40	45	49
Crystal System	Tetragonal					
Space Group	$I4/mcm$					
Z	8					
a (Å)	6.215(3)	6.1094(16)	6.0887(19)	6.062(4)	6.0106(13)	5.9885(13)
c (Å)	5.1128(15)	5.0392(12)	5.0182(14)	5.010(3)	4.9539(10)	4.9343(9)
V (Å^3)	197.5(2)	188.09(11)	186.04(13)	184.1(3)	178.97(9)	176.95(8)
Data collection						
No. of reflections						
measured	277	276	269	253	232	181
unique	83	81	81	79	75	64
unique with I $> 2\sigma$	46	52	47	25	56	59
R_{int}	0.0714	0.068	0.0811	0.3762	0.0376	0.0146
Refinement						
No. of parameters	4	4	4	3	8	11
No. of restraints	0	0	0	0	0	5
Data/parameter ratio	11.5	13	11.8	8.3	7	5.4
R_1 $[I > 2\sigma(I)]$	0.1323	0.0821	0.0724	0.254	0.06	0.0321
wR_2 (all data)	0.4102	0.2151	0.1853	0.5699	0.1558	0.0855
$\Delta\rho_{min}/\Delta\rho_{max}$ (eÅ^{-3})	1.37/-1.27	1.30/-1.70	0.98/-0.93	1.86/-1.85	0.66/-0.78	0.54/-0.43

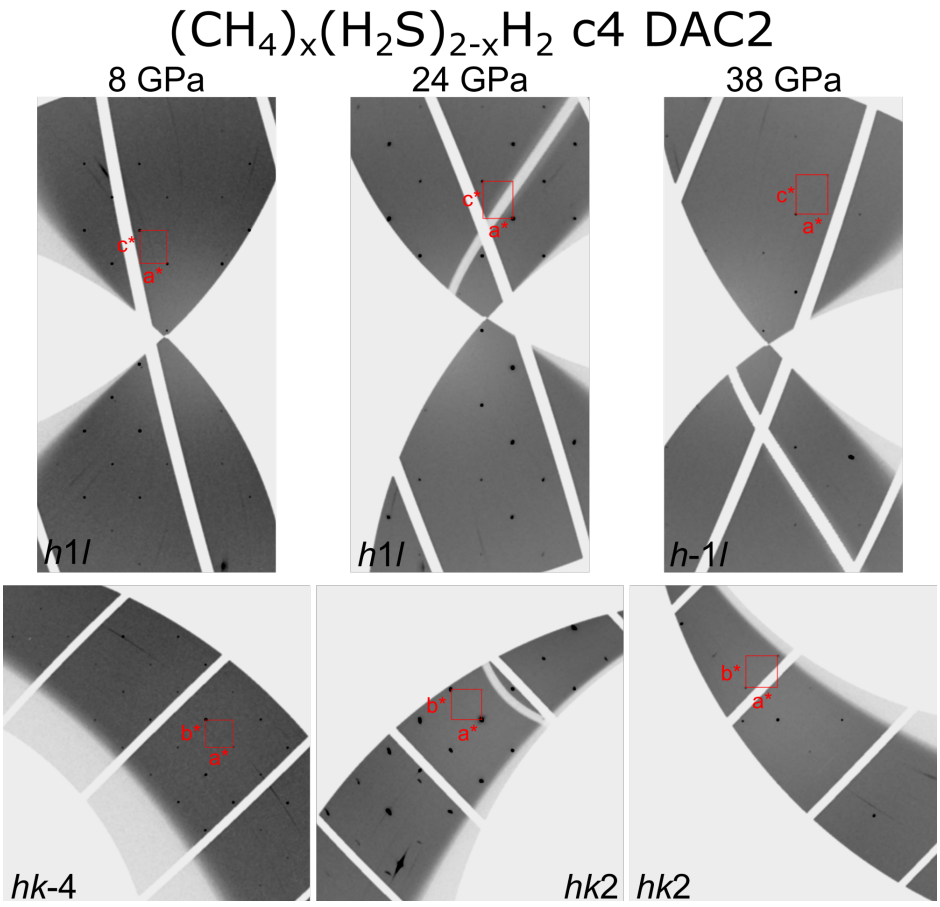

Figure S7: Selected reciprocal space reconstructions for crystal 4 of the $(CH_4)_x(H_2S)_{2-x}H_2$ loading in DAC2. No monoclinic distortion is observed at 24 GPa. Crystal alignment issues means that there are no data above 9 GPa up till 24 GPa. At 24 GPa, the position of c4 was re-defined.

$(H_2S)_2H_2$ DAC3

Table SXVII: Crystallographic details of the $(H_2S)_2H_2$ loading in DAC3. The hydrogens bonded to S were not included in the refinement.

P (GPa)	8.1	15.3	23.1	30.0	39.7	48.1
Crystal System	Tetragonal					
Space Group	$I4/mcm$					
Z	8					
a (Å)	7.035(3)	6.6313(10)	6.42(2)	6.282(5)	6.102(5)	6.018(7)
c (Å)	5.830(3)	5.5173(13)	5.39(3)	5.149(7)	4.987(10)	4.938(10)
V (Å^3)	288.5(3)	242.62(9)	221.8(19)	203.2(4)	185.7(5)	178.8(5)
Data collection						
No. of reflections						
measured	328	271	248	205	186	184
unique	140	118	105	96	90	90
unique with I $> 2\sigma$	88	99	39	71	57	61
R_{int}	0.0219	0.0493	0.0480	0.1022	0.1477	0.1535
Refinement						
No. of parameters	7	7	5	4		
No. of restraints	1	1	1	1		
Data/parameter ratio	12.6	14.1	7.8	17.8		
R_1 $[I > 2\sigma(I)]$	0.0766	0.0479	0.1105	0.2603		
wR_2 (all data)	0.1924	0.1280	0.3451	0.5617		
$\Delta\rho_{min}/\Delta\rho_{max}$ (eÅ^{-3})	0.55/−0.53	0.58/−0.65	0.95/−0.57	4.1/−2.2		

Table SXVIII: Crystallographic details of the $(H_2S)_2H_2$ loading in DAC3 at 23 GPa at position 2. No hydrogens were included in the refinement.

P (GPa)	23.1
Crystal System	Monoclinic
Space Group	$C2/c$
Z	24
a (Å)	8.321(6)
b (Å)	6.4115(11)
c (Å)	12.410(3)
β (°)	98.70(5)
V (Å^3)	654.4(5)
Data collection	
No. of reflections	
measured	801
unique	545
unique with I $> 2\sigma$	373
R_{int}	0.1166
Refinement	
No. of parameters	14
No. of restraints	0
Data/parameter ratio	26.6
R_1 $[I > 2\sigma(I)]$	0.1453
wR_2 (all data)	0.3814
$\Delta\rho_{min}/\Delta\rho_{max}$ (eÅ^{-3})	1.4/−0.77

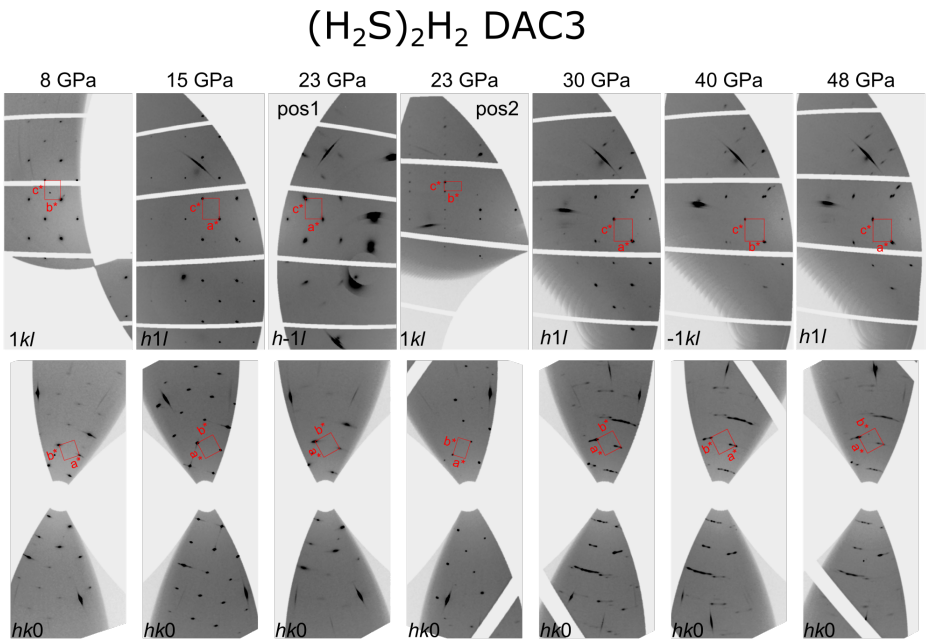

Figure S8: Reciprocal space reconstructions for $(H_2S)_2H_2$ loading in DAC3. The 23 GPa pressure point has two reconstructions in different positions of the crystal. The $C2/c$ phase is observed for position 2 at 23 GPa. The data quality significantly reduced at 30 GPa and above, where twinning and high mosaicity in the (**ab**)-plane are observed.

$(CH_4)_x(H_2S)_{2-x}H_2$ DAC4

Table SXIX: Crystallographic details of the $(CH_4)_x(H_2S)_{2-x}H_2$ loading in DAC4 at 90 GPa.

P (GPa)	90
Crystal System	Tetragonal
Space Group	$I4/mcm$
Z	8
a (Å)	5.577(4)
c (Å)	4.586(4)
V (Å^3)	142.6(2)
Data collection	
No. of reflections	
measured	62
unique	36
unique with I $> 2\sigma$	34
R_{int}	0.0163
Refinement	
No. of parameters	4
No. of restraints	0
Data/parameter ratio	9
R_1 $[I > 2\sigma(I)]$	0.1576
wR_2 (all data)	0.3904
$\Delta\rho_{min}/\Delta\rho_{max}$ (eÅ^{-3})	2.2/−1.78

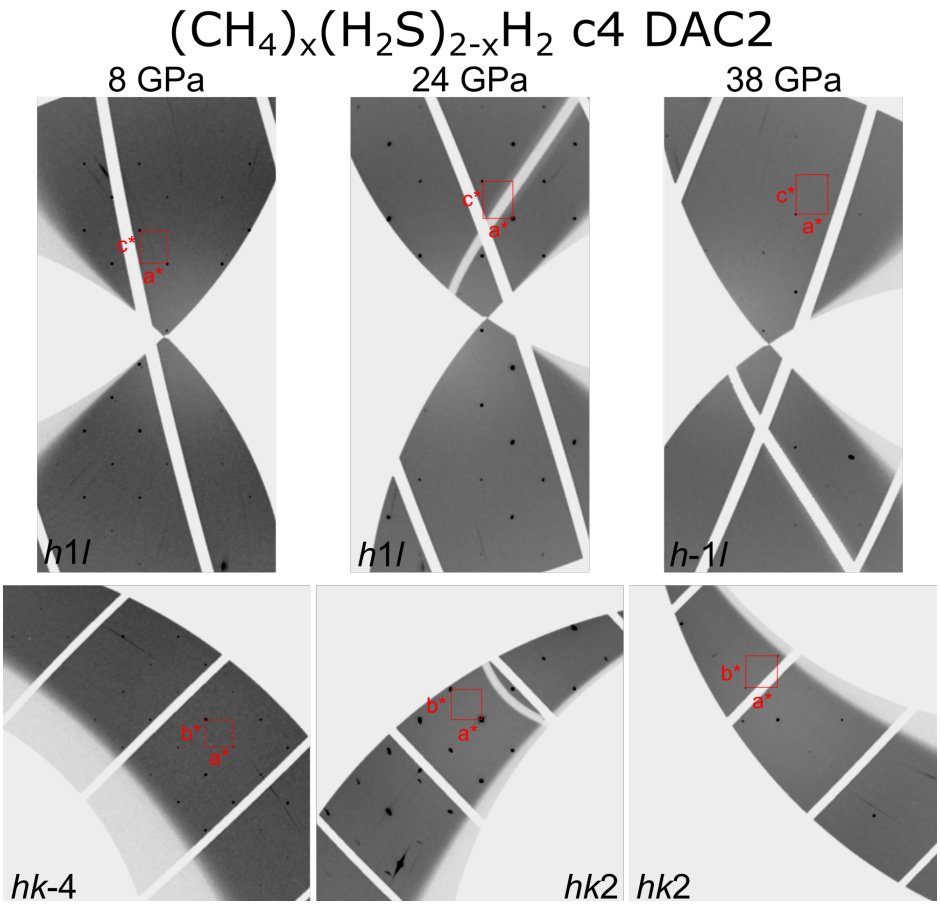

Figure S9: Reciprocal space reconstructions for $(CH_4)_x(H_2S)_{2-x}H_2$ loading in DAC4 at 90 GPa. Two twin domains are present, and each twin has additional weaker reflections visible in the diagonal of the **ab**-plane, which could be modelled using an incommensurate modulation **q*** vector as 0.241(5) 0.237(5) 0(0.005).

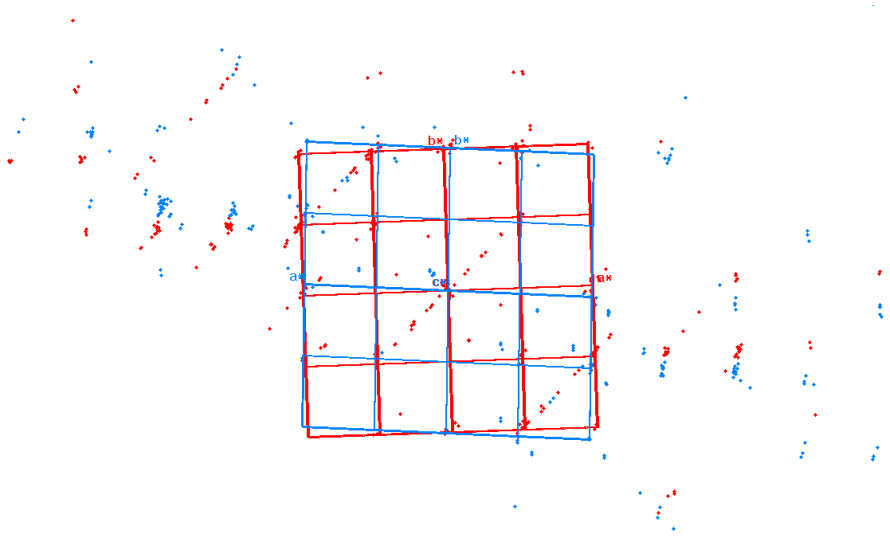

Figure S10: Reflections from the two twin domains (red and blue) with the incommensurate peaks from each domain.

Hydrogen positions

The positions of the hydrogens were located from the difference Fourier maps for the single-crystal data collections with the best integration statistics. Figure 11 shows the steps in the refinement when the H positions were added. We note that the positive electron density in Figure 11(a) is located at the center of the H_2 bonding. Indeed molecular dynamics simulations indicate that the H_2 molecule is freely rotating about the central $4c$ Wykoff site. In Figure 11(b), the distance between the S atom and the positive electron density is at 1.35 Å, which matches well with the expected S–H bonding distance. Figure 11(c) illustrates that the occupancy of the H position bonded to S is not fully occupied, and the next refinement step with a halved H occupancy results in a better residual $F_o - F_c$ map. Addition of the remaining H positions does not result in significant changes in the R factors, although the difference map does improve (Figure 11(g,h)).

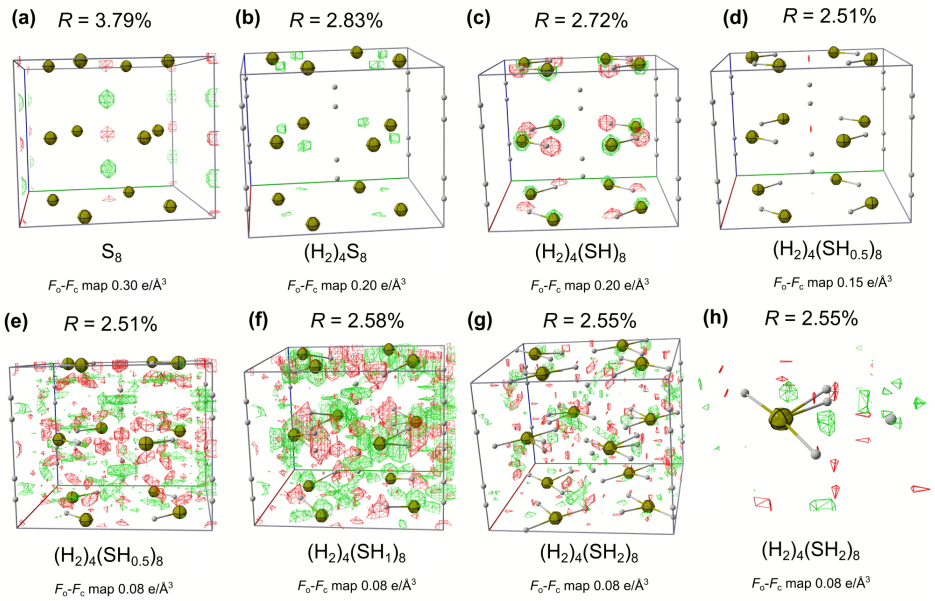

Figure S11: Figures illustrating how the hydrogen positions were allocated starting from S_8 for c3 at 12.2 GPa. The difference Fourier maps ($F_o - F_c$) are shown at the levels indicated below each figure.

The same procedure described above was applied to c1 at the pressure point 14.4 GPa (Figure 12). The difference Fourier maps are shown for each addition of H, which is initially incorporated as fully occupied. The following step involved halving the H occupancy bonded to S.

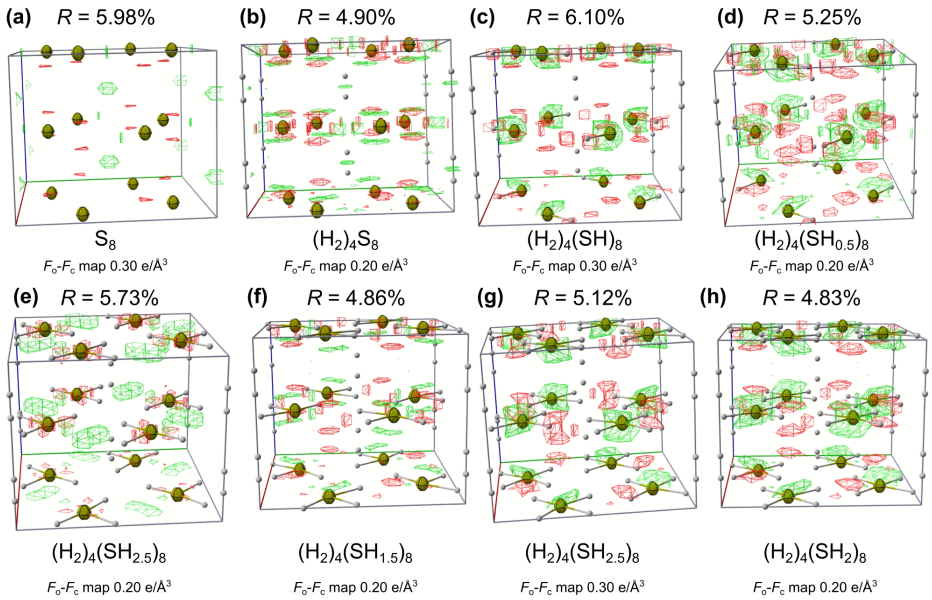

Figure S12: Figures illustrating how the hydrogen positions were allocated starting from S_8 for c1 at 14.3 GPa. The difference Fourier maps ($F_o - F_c$) are shown at the levels indicated below each figure.

EXTENDED TRANSPORT DATA

Presented below are the T_C measurements for the Run T2 performed in this work

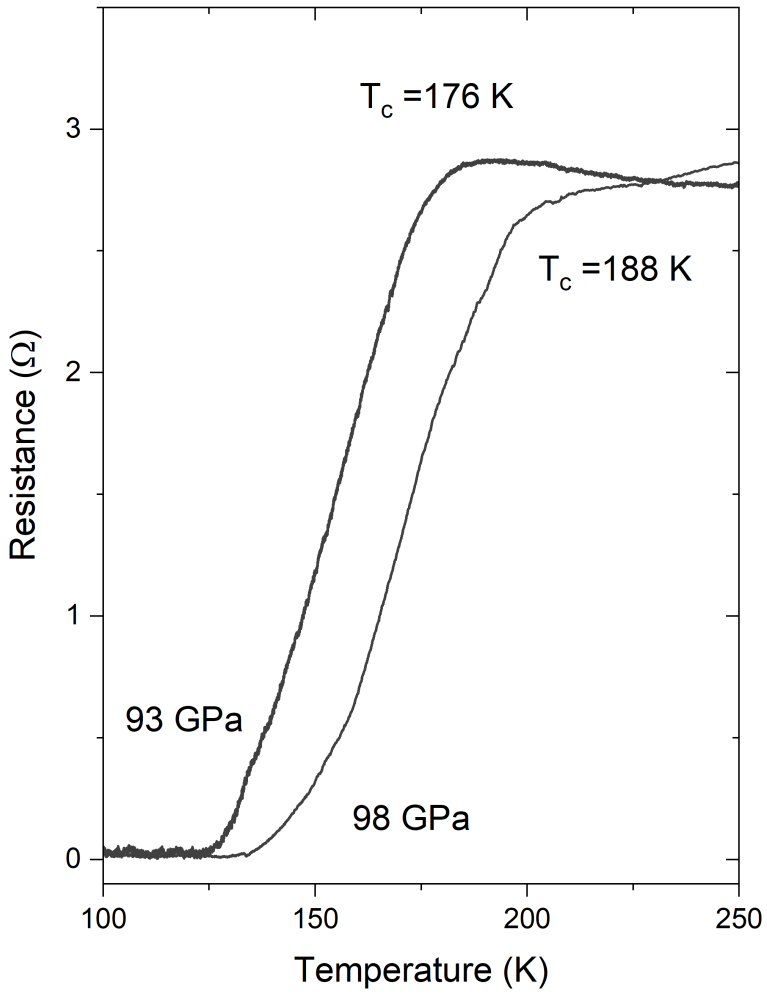

Figure S13: Resistance response with temperatures for run 2 of the transport data

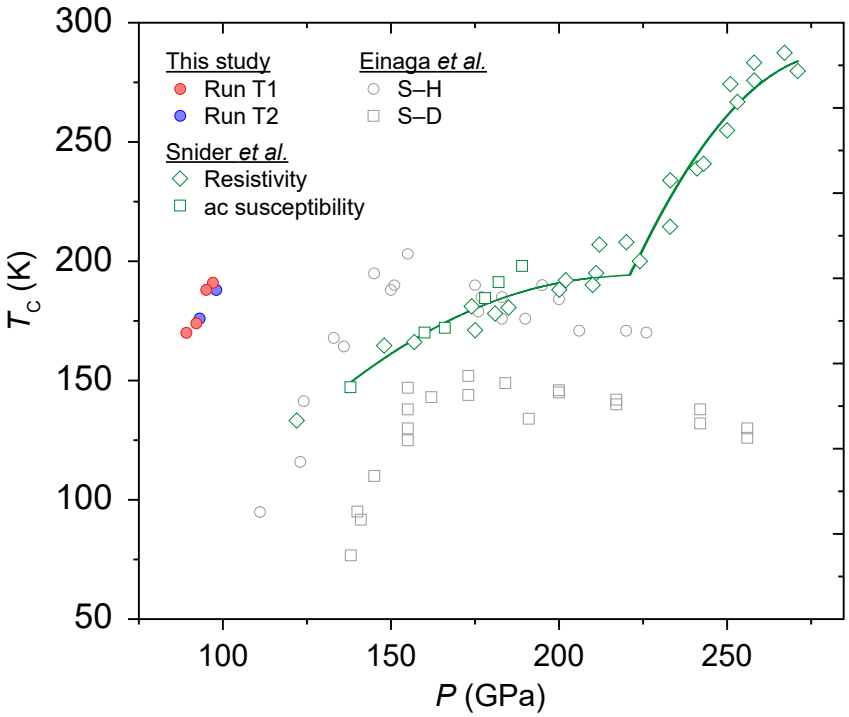

Figure S14: A comparison of the critical temperatures presented in this work with C-S-H from Snider *et al.* [1] and SH_3 from Einaga *et al.* [9]

Table SXX: $\Delta T/T_C$ Values for runs T1 and T2. Values were calculated by normalizing Resistance over the superconducting transition and taking values between 90% and 10% of the transition. Also provided are the resistance values used to normalize each measurement.

Run	P (GPa)	ΔT (K)	Resistance (Ω)	Tc (K)	DT/TC
T1	89	12	1.574	170	0.0706
	92	10.8	0.802	174	0.0621
	95	14.8	0.867	188	0.0787
	97	7.2	0.743	191	0.0377
T2	93	39.2	2.866	176	0.223
	98	44.4	2.759	188	0.236

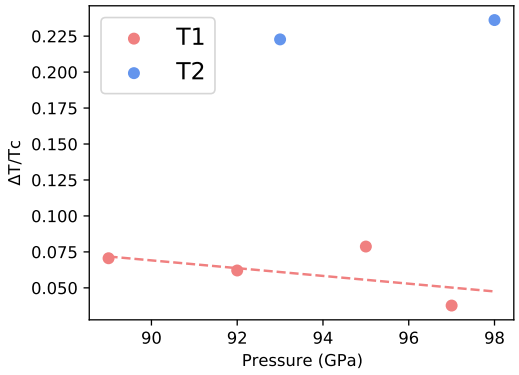

Figure S15: The $\Delta T/T_C$ values for runs T1 and T2 with pressure. Run T1 displays a much narrower transition than T2, which has a near three times broader transition. A least-squares trendline was added to the T1 data as a guide to the eye.

SIMULATIONS

Plane-wave density functional theory (PW-DFT) *ab initio* simulations were performed with the Vienna *ab initio* simulation package (VASP) version 5.4.4 using the vdW-DF2 non-local correlation functional.[10] The simulations used an evenly space Γ–centered k-point grid with 0.2 $Å^{-1}$ resolution.[11] As the system is potentially metallic, the Brillouin zone was integrated using Gaussian smearing with a width of 0.15 eV. The basis set cutoff energy was 800 eV using the projector augmented wave (PAW) [12] pseudo-potentials formulated for PBE based GW simulations (version 5.4) with valence configurations of $3s^2 3p^4$ for S, $2s^2 2p^2$ for C, and the "hard" 1s for H (ie. H_h_GW). The self-consistent field simulations were converged to 1E-6 eV and forces in optimizations were converged to 1E-3 $eVÅ^{-1}$. Optimizations of the atomic positions were performed with the lattices and sulfur positions fixed at their experimentally determined values unless otherwise noted.

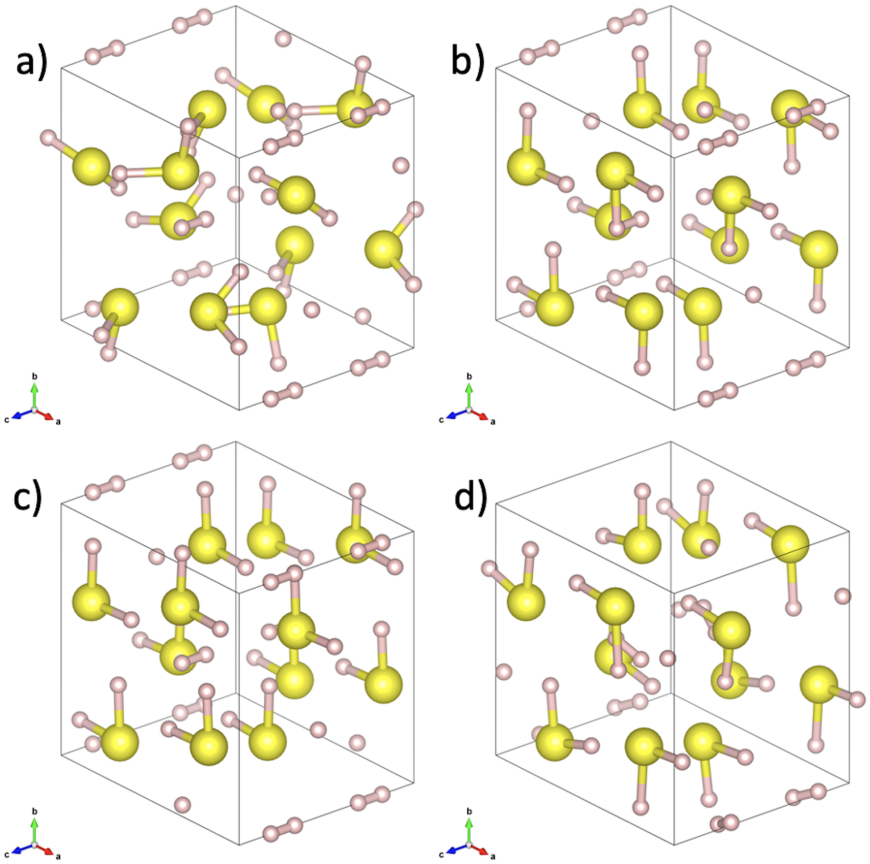

Figure S16: 4 possible arrangements of the H_2S units within the refined 50 GPa $I4/mcm$ structure with the lattice and S positions fixed at their refined positions (Fig. 3c of the main text), and using the H positions of the (a) $P1$ structure of Duan *et al.* [13] or (b-d) constructed from the partial occupancies refined here. Each (b-d) structure was constrained to obey the ice rules and is an example of a class of arrangements with (b) being rings of stacked pinwheels pointed the same direction, (c) being linear chains in [100] with each molecular unit pointed the same direction, and (d) being linear chains along [001] with each molecular unit pointed the same direction.

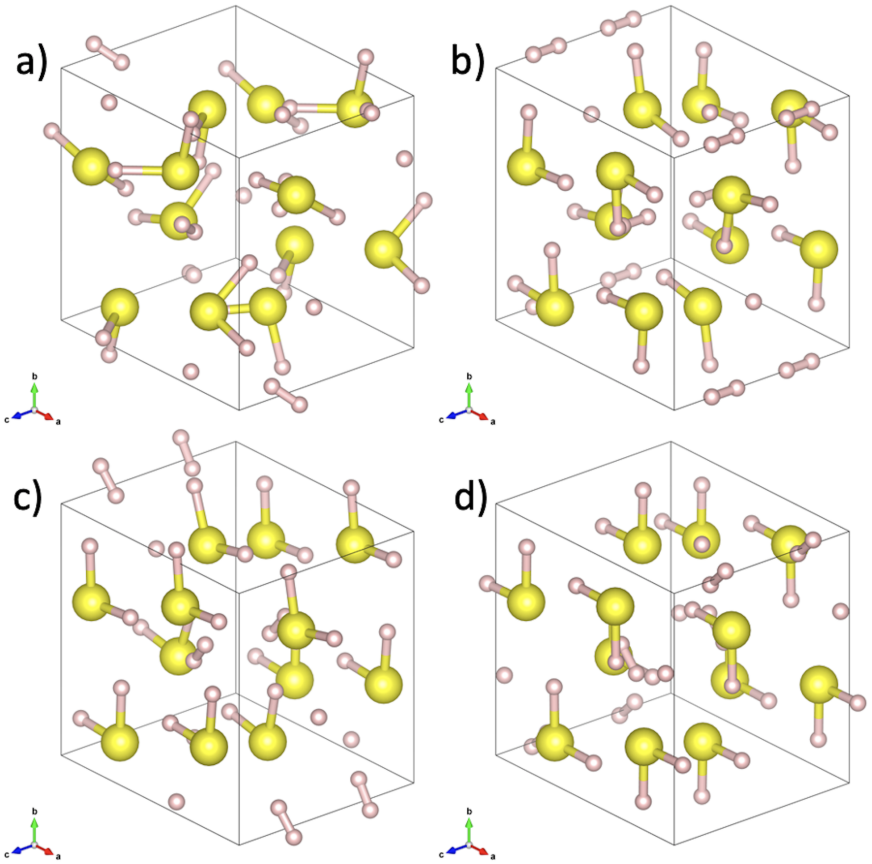

Figure S17: The optimized versions of the 50 GPa $I4/mcm$ (keeping the lattice and S positions fixed at their refined positions) structures shown in Fig. S16; the (a-d) numbering is the same. Note the H_2S molecular units in (b-d) remained planar following the optimization. The relative enthalpies are: (a) 0.000 eV, (b) 6.433 eV, (c) 5.057 eV, and (d) 4.605 eV. (d) is the most stable planar structure evaluated here.

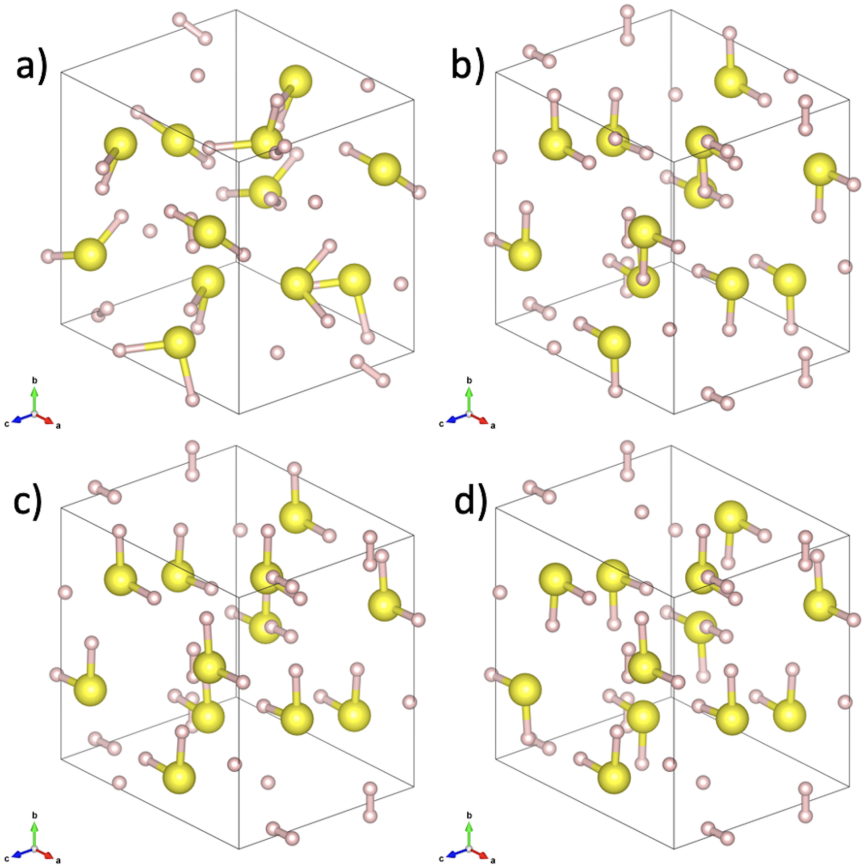

Figure S18: 4 possible arrangements of the H_2S units within the refined 9 GPa $I4/mcm$ structure with the lattice and S positions fixed at their refined positions (Fig. 3a of the main text) and using the same H arrangements and (a-d) numbering as in Fig. S16.

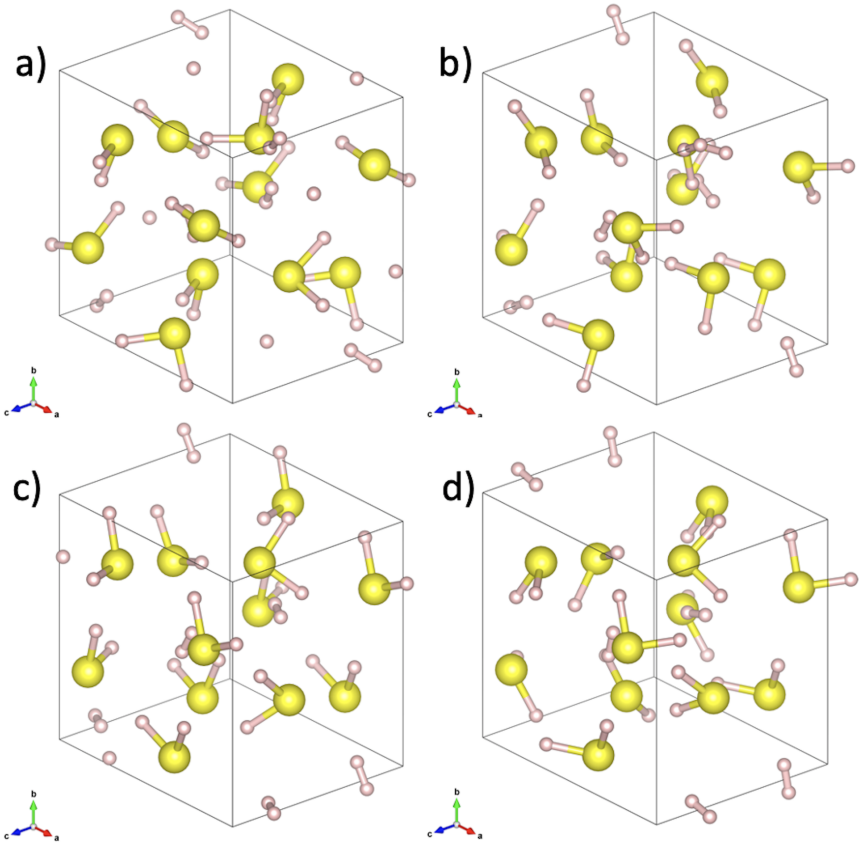

Figure S19: The optimized versions of the 9 GPa $I4/mcm$ (keeping the lattice and S positions fixed at their refined positions) structures shown in Fig. S18. The (a-d) numbering is the same. Note that some of the H_2S molecular units in each of (b-d) shifted away from being planar following the optimization. The relative enthalpies are: (a) 0.000 eV, (b) 1.136 eV, (c) 0.438 eV, and (d) 0.504 eV.

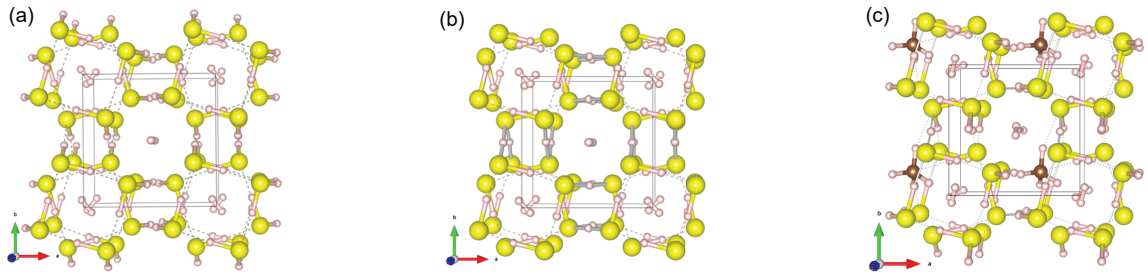

Figure S20: (a) Lowest enthalpy DFT orientation of 50 GPa $I4/mcm$ $(H_2S)_2H_2$ found here using the experimental unit cell and S positions. (b) The same configuration as (a) using the 90 GPa SC-XRD determined unit cell and S positions. (c) A higher enthalpy, $\Delta H = 267$ meV per unit cell not vibrationally corrected, solution than Figure 3(e) in the main text but with H_2S molecular orientation more akin to what was found in (b). In (a-d), bicolor cylinders represent bonds ($\leq$1.43 Å), silver single color cylinders represent H atoms shared between two heavy atoms (1.43-1.53 Å), and dashed lines represent hydrogen bonds (1.53-2.0 Å).

* ashkan.salamat@unlv.edu

[1] E. Snider, N. Dasenbrock-Gammon, R. McBride, M. Debessai, H. Vindana, K. Vencatasamy, K. Lawler, A. Salamat, and R. Dias, Nature **586**, 373 (2020).

[2] G. Shen, Y. Wang, A. Dewaele, C. Wu, D. E. Fratanduono, J. Eggert, S. Klotz, K. F. Dziubek, P. Loubeyre, O. V. Fatyanov, P. D. Asimow, T. Mashimo, R. M. M. Wentzcovitch, and other members of the IPPS task group, High Pressure Research **40**, 299 (2020).

[3] D. Smith, D. P. Shelton, P. B. Ellison, and A. Salamat, Rev. Sci. Instrum. **89**, 103902 (2018).

[4] C. Prescher and V. B. Prakapenka, High Pressure Res. **35**, 223 (2015).

[5] "Rigaku oxford diffraction, crysalispro software system, version 171.40.64.67a, rigaku corporation, oxford, uk.".

[6] G. M. Sheldrick, Acta Cryst. A **71**, 3 (2015).

[7] G. Sheldrick, Acta Cryst. A **64**, 112 (2008).

[8] C. B. Hübschle, G. M. Sheldrick, and B. Dittrich, J. Appl. Crystallogr. **44**, 1281 (2011).

[9] M. Einaga, M. Sakata, T. Ishikawa, K. Shimizu, M. Eremets, A. Drozdov, I. Troyan, N. Hirao, and Y. Ohishi, Nature Phys **12**, 835 (2016).

[10] K. Lee, E. D. Murray, L. Kong, B. I. Lundqvist, and D. C. Langreth, Phys. Rev. B **82**, 081101 (2010).

[11] J. D. Pack and H. J. Monkhorst, Phys. Rev. B **16**, 1748 (1977).

[12] P. E. Blöchl, Phys. Rev. B **50**, 17953 (1994).

[13] D. Duan, Y. Liu, F. Tian, D. Li, X. Huang, Z. Zhao, H. Yu, B. Liu, W. Tian, and T. Cui, Sci. Rep. **4**, 6968 (2014).